Multiexcitons in flexible Rydberg aggregates

G. Abumwis[1,2] and S. Wüster[1,3,*]

[1]*Department of Physics, Bilkent University, Ankara 06800, Turkey*
[2]*Max Planck Institute for the Physics of Complex Systems, Nöthnitzer Strasse 38, 01187 Dresden, Germany*
[3]*Department of Physics, Indian Institute of Science Education and Research (IISER) Bhopal, Madhya Pradesh, 462066, India*

Flexible Rydberg aggregates, assemblies of a few Rydberg atoms coherently sharing electronic excitations while undergoing directed atomic motion, show great promise as a quantum simulation platform for nuclear motion in molecules or quantum energy transport. Here we study additional features that are enabled by the presence of more than a single electronic excitation, thus considering multiexciton states. We describe cases where these can be decomposed into underlying single-exciton states and then present dynamical scenarios with atomic motion that illustrate exciton-exciton collisions, exciton routing, and strong nonadiabatic effects in simple one-dimensional settings.

I. INTRODUCTION

Ultracold Rydberg atoms are now recognized as a promising tool for scalable neutral atom quantum information [1], quantum nonlinear optics [2–5] or the simulation of condensed-matter systems [6–9]. In such applications, the thermal or interaction-induced motion of atoms gives rise to detrimental but unavoidable noise sources [10,11]. This problem is turned into an asset when using Rydberg atoms for the quantum simulation of nuclear dynamics in complex molecules, within flexible Rydberg aggregates [12], where Rydberg atomic motion replaces nuclear motion albeit on much larger and more accessible length scales.

If desired, Rydberg atoms can be easily put into motion, either by van der Waals interactions or the more interesting dipole-dipole interactions [13,14]. This motion is then governed by Born–Oppenheimer (BO) surfaces that lead to dynamics of repulsive, attractive, or indeterminate nature, depending on the overall electronic state of the Rydberg system [12,15]. Earlier work has shown interesting interplay between excitation transport and this atomic motion even in simple one-dimensional settings [16–18].

These studies have so far been restricted to cases where a single excitation in an angular-momentum p ($l = 1$) state is undergoing transport on a backbone of Rydberg atoms that are otherwise in s ($l = 0$). Here we present initial investigations of the more complex case, where multiple p excitations are present. This will lead to a larger variety of dipole-dipole BO surfaces that can be designed. While the experimental excitation of Rydberg aggregates with precisely one excitation is in principle straightforward [17,19], there will always be a small probability of multiple excitation that further motivates our studies. Additionally, multiexciton states have been thoroughly studied in molecular aggregates, especially in light-harvesting complexes [20,21]. Thus, by accessing multiexciton states, we widen the scope of Rydberg aggregates for the quantum simulation of light harvesting [22].

We show that multiexciton scenarios can be treated formally in a similar way to those containing a single exciton, initially demonstrating how for specific cases the spectrum of two-exciton states can be obtained by a decomposition into single-exciton states. However, in general, this decomposition will be limited. When considering atomic motion due to multi-excitonic BO surfaces, we focus on several examples that highlight key scenarios beyond those explorable within the single excitation manifold, such as the interaction of two excitation pulses, excitation transport switching, and strong nonadiabatic effects for one-dimensional motion.

This article is organized as follows: In section II, we introduce a theoretical description of bi-excitons in one-dimensional Rydberg aggregates. Next, in Sec. III we compare bi-excitons with excitons for two cases and show when bi-excitons can be written as product states of excitons. Then, in Sec. IV, we proceed to discuss the induced motion of atoms in the aggregate and its dependence on the initial state. In Sec. V we look into the mutual interplay between the motional and electronic dynamics, where we highlight a number of emerging scenarios that are exclusive to bi-excitons. We show that two exciton pulses undergo elastic repulsive collisions (Sec. V A), illustrate the possibility of switching or gating one exciton pulse by another (Sec. V B), and finally identify a special case with particularly prominent effects of nonadiabatic transitions on the dynamics (Sec. V C).

II. MULTIEXCITONS

We consider a chain of N identical Rydberg atoms that are confined to move in one dimension, with atomic positions described by $\mathbf{R} = (\mathbf{r}_1, \mathbf{r}_2, \mathbf{r}_3 \ldots)$ where $\mathbf{r}_n$ denotes the position of the nth atom; see Fig. 1. Each atom on the chain is initially prepared in one of two energetically close Rydberg states: a lower state $|s\rangle$ with energy ε_s or a higher state $|p\rangle$ with ε_p such that $\varepsilon_p > \varepsilon_s$. The single-exciton manifold with exactly one
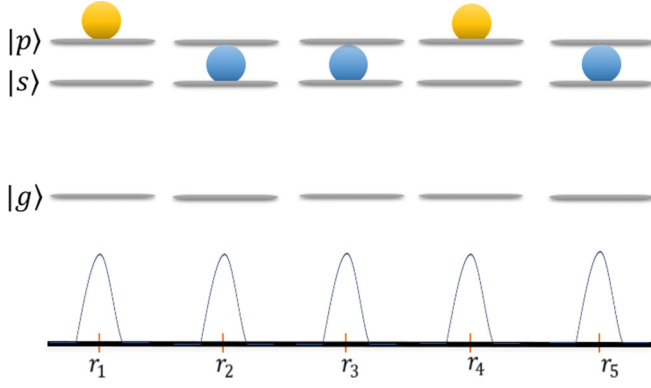
*sebastian@iiserb.ac.in

FIG. 1. (top) Essential state diagram of a Rydberg aggregate, illustrating the state $|\pi_{14}\rangle$; see text. (bottom) Corresponding atomic positions and position uncertainties.

FIG. 2. Representation of all bi-exciton states ζ_k for case (i), a homogenous chain with separation $d = 5$ μm of five Rydberg atoms ($N = 5$) with $q = 2$ excitations. The atomic locations are sketched at the top. The color indicates the amplitude $c_{k;nm}$ (see text), and the row (column) of the tiles the indices n (m) of p excited atoms.

atom in a p state and all others in the s state is then spanned by the basis $|\pi_n\rangle = |n\rangle = |sss \cdots p \cdots sss\rangle$, where in state $|\pi_n\rangle$ only the nth atom is in p. To generalize the notation to q excitations, we employ the basis $|\Pi_j^{(q)}\rangle = |n_j m_j \cdots l_j\rangle$, where $\{n_j, m_j, \cdots l_j\}$ are a set of $\bar{N} = \binom{N}{q}$ integers that indicate which q atoms carry the p excitations. The index j is just numbering the possible combinations, and thus runs from $1, \ldots, \bar{N}$. For example, in the case of two p excitations we have $|\Pi_1^{(2)}\rangle = |1, 2\rangle$, $|\Pi_2^{(2)}\rangle = |1, 3\rangle$, to $|\Pi_{10}^{(2)}\rangle = |4, 5\rangle$.

A. Hamiltonian

The Hamiltonian constrained to the single-exciton state space is

$$\mathcal{H}_{\text{el}}^{(1)}(\mathbf{R}) = \sum_{n,m:n\neq m}^{N} \frac{C_3}{R_{nm}^3} |\pi_n\rangle\langle\pi_m| - \mathbb{1} \sum_{l,k:l\neq k}^{N} \frac{C_6}{2R_{lk}^6}, \quad (1)$$

with $R_{nm} = |\mathbf{r}_n - \mathbf{r}_m|$ being the distance between atoms n and m. The operator $\mathbb{1} = \sum_n^N |\pi_n\rangle\langle\pi_n|$ is the identity in electronic space. C_3 and C_6 are the dispersion coefficients for resonant dipole-dipole and van der Waals (VdW) interactions, respectively, where for the latter we assume equal interactions for ss and sp pair states for simplicity.

In this article we mainly focus on the case of exactly two p excitations for which we can write

$$\mathcal{H}_{\text{el}}^{(2)}(\mathbf{R}) = \sum_{i,j:i\neq j}^{\bar{N}} V_{ij}(\mathbf{R}) |\Pi_i^{(2)}\rangle\langle\Pi_j^{(2)}| - \mathbb{1} \sum_{l,k:l\neq k}^{N} \frac{C_6}{2R_{lk}^6}, \quad (2)$$

where $\bar{N} = \binom{N}{2}$, $|\Pi_i^{(2)}\rangle = |n_i m_i\rangle$, and

$$V_{ij}(\mathbf{R}) = \left(\delta_{m_i m_j} \frac{C_3}{R_{n_i n_j}^3} + \delta_{n_i n_j} \frac{C_3}{R_{m_i m_j}^3} + \delta_{m_i n_j} \frac{C_3}{R_{n_i m_j}^3} \right.$$

$$\left. + \delta_{n_i m_j} \frac{C_3}{R_{m_i n_j}^3} \right). \quad (3)$$

The notation could be straightforwardly generalized to more than two excitations ($q > 2$), but this will not be needed here.
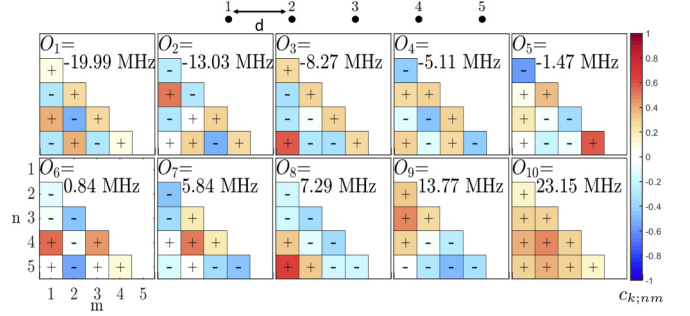
B. Excitons

We call the eigenstates of the interacting Hamiltonians above (Frenkel) excitons [23]. For later use, we distinguish solutions of the single-excitation eigenproblem

$$\mathcal{H}_{\text{el}}^{(1)}|\varphi_k^N(\mathbf{R})\rangle = U_k(\mathbf{R})|\varphi_k^N(\mathbf{R})\rangle \quad (4)$$

from those for two excitations

$$\mathcal{H}_{\text{el}}^{(2)}|\zeta_k^N(\mathbf{R})\rangle = O_k(\mathbf{R})|\zeta_k^N(\mathbf{R})\rangle. \quad (5)$$

We keep the number of Rydberg atoms N as an additional labeling parameter and $U_k(\mathbf{R})$ [$O_k(\mathbf{R})$] are the exciton energies (Born–Oppenheimer surfaces [12]) for the one-excitation (two-excitation) case. Accordingly, $|\varphi_k^N(\mathbf{R})\rangle$ [$|\zeta_k^N(\mathbf{R})\rangle$] are the exciton eigenstates.

III. BI-EXCITON VERSUS SINGLE-EXCITON STATES

We first contrast bi-exciton states with single-exciton states for two simple cases: (i) a regular chain with equal distance between neighboring atoms set at $d = 5$ μm, as shown in Fig. 1, and (ii) a chain with a dislocation at one end, where the final atom is distance of only $a = d/2$ from its neighbor. For both cases we solve Eq. (5) and refer to Ref. [15] for the solutions of Eq. (4).

These bi-exciton states have the structure $|\zeta_k^5(\mathbf{R})\rangle = \sum c_{k;nm}|nm\rangle$, and we show the coefficients $c_{k;nm} = \langle nm|\zeta_k^5(\mathbf{R})\rangle$ for their visualization. For the homogenous chain [case (i)] these are shown in Fig. 2. As required by symmetry, all modes are either symmetric or antisymmetric about the center of the chain and share the properties that the excitations are fully delocalized over the chain. For the illustrative exciton energies shown we assumed $C_3 = 976$ MHz μm^3, $C_6 = 5400$ MHz μm^6, roughly corresponding to Rydberg states with a principal quantum number $\nu \approx 40$. At this separation, VdW interactions play a minor role for exciton states.

It is easier to interpret bi-exciton states and link them to single-exciton states for the dislocated chain [case (ii)] shown in Fig. 3. In this case, the dipole-dipole interaction strength between the two atoms in the dislocation, given by $C_3/|\mathbf{r}_4 - \mathbf{r}_5|^3$, provides by far the largest matrix elements in the Hamiltonian. Because of this, six of the states factor into simple tensor products
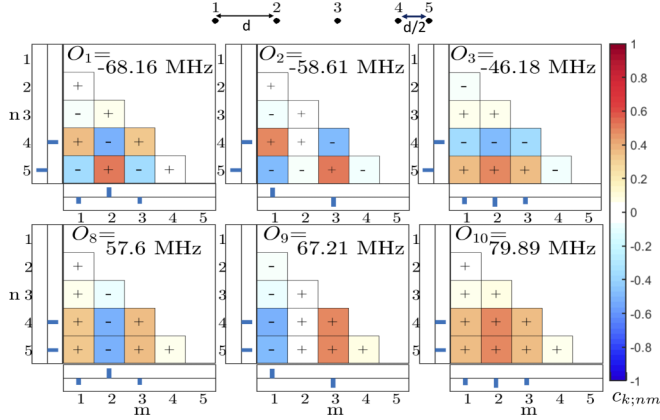
FIG. 3. Decomposition of bi-excitons into products of single-exciton states for case (ii), the dislocated chain with of five Rydberg atoms ($N = 5$). The atomic locations are sketched at the top, the base separation is $d = 5$ μm and the dislocation $a = 2.5$ μm. We show the six cases that are a simple product of two single-exciton states. The color indicates the amplitude $c_{k;nm}$ (see text), and the row (column) of the tiles the indices n (m) of p excited atoms. Bordering the tiles we show the exciton state on the dislocation (atoms 4, 5, y axis) and the remainder of the chain (atoms 1–3, x axis), where length and direction of the stick qualitatively indicate $c_{k;n}$ (see text).

of one single-exciton state for the dislocation and a second for the remainder of the chain. Specifically, we find $|\zeta_1^{(5)}\rangle = |\varphi_1^{(3)}\rangle \otimes |\varphi_1^{(2)}\rangle$, $|\zeta_2^{(5)}\rangle = |\varphi_2^{(3)}\rangle \otimes |\varphi_1^{(2)}\rangle$, $|\zeta_3^{(5)}\rangle = |\varphi_3^{(3)}\rangle \otimes |\varphi_1^{(2)}\rangle$, $|\zeta_8^{(5)}\rangle = |\varphi_1^{(3)}\rangle \otimes |\varphi_2^{(2)}\rangle$, $|\zeta_9^{(5)}\rangle = |\varphi_2^{(3)}\rangle \otimes |\varphi_2^{(2)}\rangle$, and $|\zeta_{10}^{(5)}\rangle = |\varphi_3^{(3)}\rangle \otimes |\varphi_2^{(2)}\rangle$, where the single-exciton states have the structure $|\varphi_k\rangle = \sum c_{k;n}|n\rangle$ and the coefficients $c_{k;n}$ are visualized as bars in Fig. 3. In the list above, the state to the left of the tensor product $\otimes$ pertains to atoms 1–3 (chain) and the state to the right pertains to atoms 4 and 5 (dislocation). To give one example of this tensor product notation, the state $|\zeta_1^{(5)}\rangle$ is very well approximated by

$$
\begin{aligned}
|\zeta_1^{(5)}\rangle &= -|\varphi_1^{(3)}\rangle \otimes |\varphi_1^{(2)}\rangle \\
&= \left(\frac{1}{2}|\pi_1\rangle - \frac{1}{\sqrt{2}}|\pi_2\rangle + \frac{1}{2}|\pi_3\rangle\right) \otimes \frac{1}{\sqrt{2}}(|\pi_4\rangle - |\pi_5\rangle) \\
&= \frac{1}{2\sqrt{2}}(|14\rangle - \sqrt{2}|24\rangle + |34\rangle - |15\rangle \\
&\quad + \sqrt{2}|25\rangle - |35\rangle).
\end{aligned}
\tag{6}
$$

In the last line we used the states $|\Pi^{(2)}\rangle$ defined in Sec. II.

There are also four states that cannot be reduced to known single-exciton results, shown in Fig. 4. These can be understood as the state with both p excitations on the dislocation, and three states where both p excitations avoid the dislocation and reside on the main chain. In the latter three cases, these then form essentially single-exciton states on the main chain, for which the role of the s and p electronic levels are inverted. These can be written in a basis $|\bar{\pi}_n\rangle = |ppp\cdots s\cdots pppp\rangle$, where in this state all atoms are in p except the nth atom, which is in s. Writing the corresponding inverted exciton states as $|\bar{\varphi}_k\rangle$, we can write $|\zeta_4^{(5)}\rangle = |\bar{\varphi}_1^{(3)}\rangle \otimes$
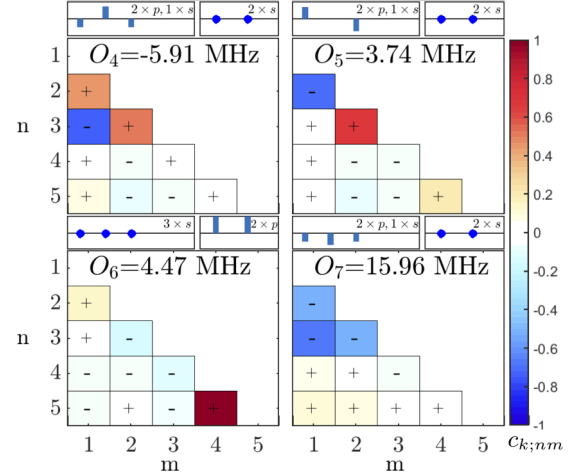

FIG. 4. Special bi-exciton states that cannot be decomposed into single exciton ones. The labeling is as in Figs. 2 and 3.

$|ss\rangle$, $|\zeta_5^{(5)}\rangle = |\bar{\varphi}_2^{(3)}\rangle \otimes |ss\rangle$, $|\zeta_7^{(5)}\rangle = |\bar{\varphi}_3^{(3)}\rangle \otimes |ss\rangle$, and $|\zeta_6^{(5)}\rangle = |sss\rangle \otimes |pp\rangle$.

IV. ATOMIC MOTION IN A FLEXIBLE RYDBERG AGGREGATE

The dipole-dipole-induced motion of atoms in a flexible bi-exciton aggregate could be studied by solving the time-dependent Schrödinger equation

$$
i\hbar\frac{\partial}{\partial t}\Psi(\mathbf{R}, t) = \left(-\frac{\hbar^2}{2m}\sum_{n=1}^{N}\nabla_n^2 + \mathcal{H}_{\text{el}}^{(q)}(\mathbf{R})\right)\Psi(\mathbf{R}, t), \tag{7}
$$

for atoms of mass m. Even when restricting the motion of atoms to one dimension, as we will do in the following, the direct solution of Eq. (7) for $N = 5$ would be too challenging. Hence we resort to quantum-classical propagation, where the motion of atoms is treated classically. This works very well for flexible Rydberg aggregates [12,16,24].

Expanding the electronic quantum states as $|\Psi(t)\rangle = \sum c_{nm}(t)|nm\rangle$, we thus solve

$$
i\hbar\frac{\partial}{\partial t}c_{nm}(t) = \sum_{kl}\langle nm|\mathcal{H}_{\text{el}}^{(q)}(\mathbf{R})|kl\rangle c_{kl}(t), \tag{8}
$$

which is coupled to the motion of atoms

$$
\mathbf{F} = M\ddot{\mathbf{R}} = -\nabla_{\mathbf{R}}O_{\gamma(t)}(\mathbf{R}). \tag{9}
$$

Here, $\gamma(t)$ is a stochastically varied index that describes on which BO surface the system is currently evolving. The stochastic jumps between surfaces correspond to nonadiabatic transitions between exciton states. The likelihood of a transitions from surface i to surface k is set by the nonadiabatic coupling vector $\mathbf{d}_{ki} = \langle \zeta_k^{(N)}\nabla_R\phi_i^{(N)}\rangle$. All results shown are then averaged over a set of N_{traj} trajectories, typically starting from a chosen initial BO surface, i.e., $\gamma(t = 0) = k_{\text{ini}}$.

For further details on this Tully's fewest switching algorithm, we refer to the original chemical physics literature [25–27], the review [28], or our earlier work [17,29].

To obtain a first idea of the allocation of motional dynamics to an exciton state, we can proceed as in Ref. [15] and
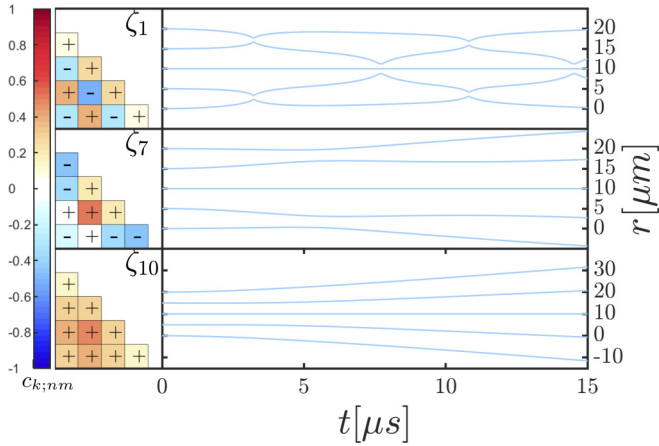
FIG. 5. Repulsive versus attractive atomic motion for selected bi-exciton states. The electronic aggregate states are shown on the left, in the same style as in Fig. 2, and are forced to be constant in time. The right panels show the evolving positions of the five atoms under the influence of the force corresponding to the Born–Oppenheimer surface that corresponds to the aggregate state in the same row on the left.
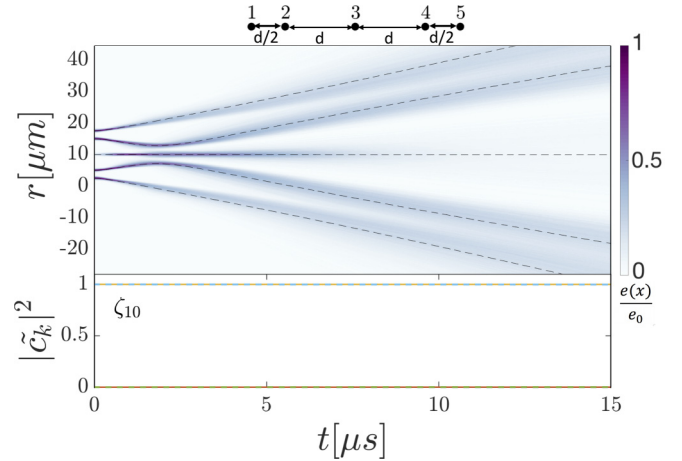

FIG. 6. Elastic collision of two excitation carrying pulses of atomic motion. (top) Mean positions of the atoms (dashed black line) on top of the weighted excitation density $e(r, t)$ (color shade). The latter represents a spatial binning of all atomic positions, each weighted with the probability to carry any excitation; see also Ref. [29]. With e_0 we denote $\max_{r,t} e(r, t)$. (bottom) Adiabatic populations $|\tilde{c}_k|^2$, where $\tilde{c}_k(t) = \langle \zeta_k(\mathbf{R}(t))|\Psi(t)\rangle$. Only $|\tilde{c}_{10}|^2$ for the initial repulsive surface is visibly nonzero, indicating essentially adiabatic dynamics. The initial repulsive state has the same character as $|\zeta_{10}\rangle$ in Fig. 2, but with suppressed population on the center atom.

initially ignore the evolution of the electronic state (8), fix $\gamma = k$ as constant in time, and thus just obtain the Newtonian motion on a fixed BO surface, as shown in Fig. 5. We see that, as for single-excitation aggregates, the type of motion is set by the overall aggregate electronic states. As usual, opposite-amplitude signs between neighboring atoms result in attractive dynamics, while the same sign results in repulsive dynamics (for $C_3 > 0$). The bounces for the attractive case result from repulsive van der Waals interactions at very short distances, which are independent of the exciton state. VdW interactions thus preclude a likely ionizing close encounter of Rydberg atoms, which is why we included them in the model. The parameters for these simulations and the following ones are as listed in Sec. III, for ^{7}Li atoms of mass 10^{-26} kg.

V. INTERPLAY OF MOTIONAL AND ELECTRONIC DYNAMICS

For a more complete picture, we now proceed to treat the coupled electronic and motional dynamics of the flexible Rydberg aggregate, also taking into account atomic-position uncertainties and nonadiabatic transitions. To that end, we consider a system that is prepared in one of the electronic Hamiltonian eigenstates $|\zeta_k^N\rangle$, with atoms assumed to be initially optically trapped in a harmonic potential before they are released to freely move in one dimension. We thus use a Gaussian probability distribution for initial positions with a standard deviation σ (the ground-state width of the trap) and the same for initial velocities with width $\sigma_v = \hbar/(M\sigma)$. Our results are then averaged over a large number N_{traj} of trajectories. For the following numerical simulations, we used $\sigma = 0.3\ \mu$m and propagated $N_{\text{traj}} = 10^4$ trajectories. As before, the main distance between nearest neighbors is $d = 5\ \mu$m; when a dislocation is present, the distance between the two atoms forming the dislocation was $a = d/2$.

In the following we present several selected dynamical scenarios, in which the presence of a second p excitation causes the emergence of crucial additional features, compared with similar scenarios with just a single p excitation.

A. Interactions of exciton pulses

In earlier work we had shown that in a flexible Rydberg aggregate, a pulse of atomic dislocation in a regular chain, with ensuing fast motion, combined with electronic excitation exhibits particularly interesting transport properties. We had called these "exciton(-motion) pulses" in Refs. [24,29]. It can adiabatically deliver a shared excitation and the associated entanglement from one end of a chain to the other [16]. This bears some resemblance to a Davydov soliton [30,31], albeit without the restoring force prominently part of the latter. These pulses can then be split and their coherence properties controlled, e.g., by modifications of chain geometry or conical intersections [24,29].

Now, with two p excitations, we are in a position to study the interaction of two such exciton motion pulses. These are shown in Fig. 6, for a scenario where each excitation is localized at a different end of a chain, with a dislocation on both ends. As the system evolves the excitation pulses collide in the chain center, due to both pulses having repulsive character. This means that, on each dislocation (top and bottom), one p excitation is shared by the two atoms $\sim|sp\rangle + |ps\rangle$. The resultant contribution to the potential energy is then positive. Finally, when colliding at the center, repulsive vdW interactions are at play and the pulses reflect off each other. The figure shows the weighted excitation density, showing that all excitation is reflected off the center. The second panel
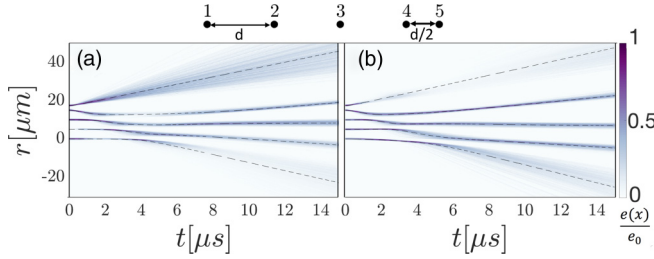
FIG. 7. Transmission gate for exciton-motion pulses. An incoming exciton motion pulse (first exciton) is reflected or transmitted depending on the exciton state of the target chain (second exciton). (a) Reflection for gate exciton in $|\varphi_2^{(5)}\rangle$. (b) Transmission for gate exciton in $|\varphi_3^{(5)}\rangle$.

indicates that the initial electronic state is being adiabatically followed with high fidelity.

B. Gate for exciton pulses

When decomposed into single-excitation states, the scenario in the previous section amounts to the collision of two exciton states of the same type, connected to the repulsive dimer state on the dislocation [15]. We now show that one exciton pulse impacting onto a chain occupied by a second excitation may be routed through the chain, or reflected off it, depending on the exciton state realized on the chain.

This is shown in Fig. 7, where the dynamics in Fig. 7(a) is initialized in state $|\zeta_9^{(5)}\rangle$ while Fig. 7(b) commences from $|\zeta_{10}^{(5)}\rangle$. Both have in common that an incoming exciton-motion pulse is associated with the dislocated atoms 1, 2 sharing one p excitation, while the second p is distributed over atoms 3–5.

According to our decomposition in Sec. III the nondislocated part of the chain is thus in the (single p) exciton state $|\varphi_2^{(5)}\rangle$ in Fig. 7(a) and $|\varphi_3^{(5)}\rangle$ in Fig. 7(b). We can see that, in Fig. 7(a), the incoming excitation is reflected off the chain, finally residing on the atom going out towards positive r, while the incoming momentum is transferred through as usual [16,17]. In contrast, for the case in Fig. 7(b), the excitation is passed through the chain together with the momentum pulse and finally resides on the atom moving out towards negative r.

While our quantum-classical approach is not able to show this, the conditional passage should even be quantum coherent if the motional wave function of the Rydberg aggregate remains quantum coherent. Note that the full-system lifetime for our parameters would be $\tau_{\text{agg}} = (2/\tau_p + 3/\tau_s)^{-1} = 19.4 \ \mu s$ for $\tau_s = 70 \ \mu s$ and $\tau_p = 232 \ \mu s$ due to spontaneous decay and blackbody redistribution at $T = 300$ K [32]. Hence we expect the motional dynamics shown to take place before the first decay of a Rydberg atom involved is to be expected.

C. Nonadiabatic transitions

Finally, we show a scenario that leads to clear and significant nonadiabatic effects even within a *one-dimensional* flexible Rydberg aggregate. Earlier, nonadiabatic effects were most prominently reported only once motion of each atom was taking place in two dimensions [24,29,33,34].

Nonadiabatic effects can be seen in Fig. 8 when starting from an electronic state akin to $|\zeta_9^5\rangle$, albeit for a doubly
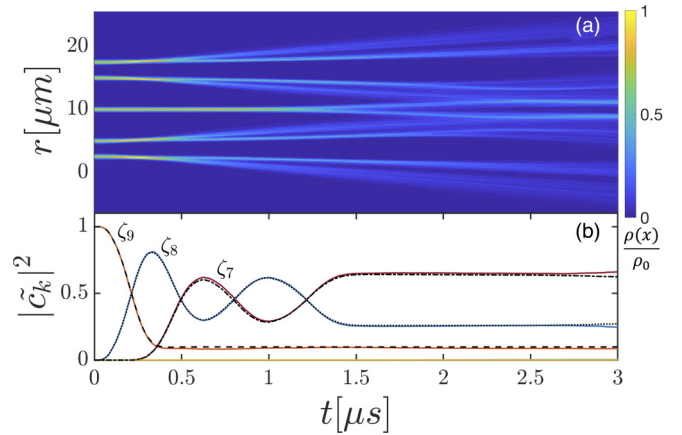

FIG. 8. Nonadiabatic evolution of a one-dimensional flexible Rydberg aggregate with two excitons. (a) Total atomic density $\rho(x, t)$ (binned atom positions) as a function of time. With ρ_0 we denote $\max_{r,t} \rho(r, t)$. Multiple spatial modes are clearly visible. (b) Adiabatic populations $\tilde{p}_k = |\tilde{c}_k|^2$ (colored lines) and matching trajectory fractions (dashed lines), indicating strong nonadiabatic effects.

dislocated chain. We notice in the total atomic density (not excitation density) shown in Fig. 8(a) that the densities for each atom start splitting around 0.5 μs, indicating a superposition occupying simultaneously multiple BO-surfaces with consequently disparate forces acting on atoms. This is corroborated by the adiabatic populations $\tilde{p}_k = |\tilde{c}_k|^2$, defined in the caption of Fig. 6 and shown here in Fig. 8(b). In contrast to the earlier scenarios, these now show large variation with ultimately three BO surfaces strongly involved in the dynamics. The figure also includes the typical consistency check for the employed quantum classical surface hopping algorithm, comparing the adiabatic populations $\tilde{p}_k(t)$ with the fraction $f_k(t)$ of trajectories currently evolving on the matching BO surface. Here $f_k(t)$ is defined as

$$f_k(t) = \frac{1}{N_{\text{traj}}} \sum_{i=1}^{N_{\text{traj}}} \delta_{k\gamma(t)}, \qquad (10)$$

where k is a chosen adiabatic surface and $\gamma(t)$ represents the adiabatic surface that the system follows as it evolves in time; see Eq. (9). We can see that surface hopping is consistent (indicating the absence of forbidden jumps), and that signatures of nonadiabaticity are visible in atomic density profiles even within this simple one-dimensional scenario, if density profiles can be measured with about 2 μm spatial resolution.

VI. CONCLUSIONS AND OUTLOOK

We have extended earlier work on flexible Rydberg aggregates from the single-excitation manifold to the two-exciton manifold. After presenting the decomposition of bi-exciton states into single-exciton states, we highlighted several dynamical features that only arise due to the addition of the second excitation. These were collisions of exciton-motion pulses, exciton pulse gates or routers controlled by the exciton state of a gate chain, as well as the occurrence of strong and

clear nonadiabatic effects in scenarios with one-dimensional motion.

Most of the scenarios shown here represent examples of joint quantum transport and electronic excitation transport that might inspire novel transport processes in devices or artificial light harvesting [35]. Multiexciton processes are of relevance in light harvesting [20,21], particularly when exciton-exciton annihilation processes are involved [36,37]. Including the latter in cold atom quantum simulations would be an interesting topic for further work.

More generally, the availability of a larger number of Born–Oppenheimer surfaces in the presence of multiple excitons enlarges the versatility of flexible Rydberg aggregates for the design of tailored BO surfaces, the principles of which are outlined in Ref. [12]. As discussed in that review, an extension to motion in two spatial dimensions typically results in more prominent conical intersections and nonadiabatic dynamics.

[1] M. Saffman, T. G. Walker, and K. Mølmer, Rev. Mod. Phys. **82**, 2313 (2010).

[2] A. K. Mohapatra, M. G. Bason, B. Butscher, K. J. Weatherill, and C. S. Adams, Nat. Phys. **4**, 890 (2008).

[3] S. Sevinçli, N. Henkel, C. Ates, and T. Pohl, Phys. Rev. Lett. **107**, 153001 (2011).

[4] T. Peyronel, O. Firstenberg, Q.-Y. Liang, S. Hofferberth, A. V. Gorshkov, T. Pohl, M. D. Lukin, and V. Vuletić, Nature (London) **488**, 57 (2012).

[5] Y. O. Dudin and A. Kuzmich, Science **336**, 887 (2012).

[6] H. Weimer, M. Müller, I. Lesanovsky, P. Zoller, and H. P. Büchler, Nat. Phys. **6**, 382 (2010).

[7] J. Zeiher, R. van Bijnen, P. Schausz, S. Hild, J. Choi, T. Pohl, I. Bloch, and C. Gross, Nat. Phys. **12**, 1095 (2016).

[8] A. W. Glaetzle, M. Dalmonte, R. Nath, I. Rousochatzakis, R. Moessner, and P. Zoller, Phys. Rev. X **4**, 041037 (2014).

[9] M. Marcuzzi, J. Minář, D. Barredo, S. de Léséleuc, H. Labuhn, T. Lahaye, A. Browaeys, E. Levi, and I. Lesanovsky, Phys. Rev. Lett. **118**, 063606 (2017).

[10] T. Wilk, A. Gaëtan, C. Evellin, J. Wolters, Y. Miroshnychenko, P. Grangier, and A. Browaeys, Phys. Rev. Lett. **104**, 010502 (2010).

[11] M. M. Müller, M. Murphy, S. Montangero, T. Calarco, P. Grangier, and A. Browaeys, Phys. Rev. A **89**, 032334 (2014).

[12] S. Wüster and J. M. Rost, J. Phys. B: At., Mol. Opt. Phys. **51**, 032001 (2018).

[13] T. F. Gallagher, *Rydberg Atoms* (Cambridge University Press, Cambridge, 1994).

[14] F. Robicheaux, J. V. Hernandez, T. Topcu, and L. D. Noordam, Phys. Rev. A **70**, 042703 (2004).

[15] C. Ates, A. Eisfeld, and J. M. Rost, New J. Phys. **10**, 045030 (2008).

[16] S. Wüster, C. Ates, A. Eisfeld, and J. M. Rost, Phys. Rev. Lett. **105**, 053004 (2010).

[17] S. Möbius, S. Wüster, C. Ates, A. Eisfeld, and J. M. Rost, J. Phys. B: At., Mol. Opt. Phys. **44**, 184011 (2011).

[18] H. Zoubi, A. Eisfeld, and S. Wüster, Phys. Rev. A **89**, 053426 (2014).

[19] S. Wüster, S. Möbius, M. Genkin, A. Eisfeld, and J.-M. Rost, Phys. Rev. A **88**, 063644 (2013).

[20] R. van Grondelle, J. P. Dekker, T. Gillbro, and V. Sundstrom, Biochim. Biophys. Acta, Bioenerg. **1187**, 1 (1994).

[21] T. Renger and V. May, Phys. Rev. Lett. **78**, 3406 (1997).

[22] D. W. Schönleber, A. Eisfeld, M. Genkin, S. Whitlock, and S. Wüster, Phys. Rev. Lett. **114**, 123005 (2015).

[23] Some confusion can arise from the varied use of (Frenkel) excitons in the condensed-matter, quantum chemistry, and molecular aggregate community. The former implies an electron-hole pair, with the hole localized on a crystal site. For a single molecule, an excited state corresponds to a Frenkel exciton with the hole in the LUMO and electron in the HOMO orbital. Finally, for molecular aggregates, Frenkel excitons imply the delocalization of the latter state over the aggregate due to interactions. Our definition is based on the analogy to the latter.

[24] K. Leonhardt, S. Wüster, and J. M. Rost, Phys. Rev. Lett. **113**, 223001 (2014).

[25] J. C. Tully, J. Chem. Phys. **93**, 1061 (1990).

[26] J. C. Tully and R. K. Preston, J. Chem. Phys. **55**, 562 (1971).

[27] S. Hammes-Schiffer and J. C. Tully, J. Chem. Phys. **101**, 4657 (1994).

[28] M. Barbatti, Wiley Interdiscip. Rev. Comput. Mol. Sci. **1**, 620 (2011).

[29] K. Leonhardt, S. Wüster, and J. M. Rost, Phys. Rev. A **93**, 022708 (2016).

[30] A. S. Davydov and N. I. Kislukha, Phys. Status Solidi B **59**, 465 (1973).

[31] W. Weidlich and W. Heudorfer, Eur. Phys. J. A **268**, 133 (1974).

[32] I. I. Beterov, I. I. Ryabtsev, D. B. Tretyakov, and V. M. Entin, Phys. Rev. A **79**, 052504 (2009).

[33] S. Wüster, A. Eisfeld, and J. M. Rost, Phys. Rev. Lett. **106**, 153002 (2011).

[34] K. Leonhardt, S. Wüster, and J. M. Rost, J. Phys. B: At., Mol. Opt. Phys. **50**, 054001 (2017).

[35] S. K. Saikin, A. Eisfeld, S. Valleau, and A. Aspuru-Guzik, Nanophotonics **2**, 21 (2013).

[36] A. Campillo, S. Shapiro, V. Kollman, K. Winn, and R. Hyer, Biophys. J. **16**, 93 (1976).

[37] B. Brüggemann and V. May, J. Chem. Phys. **120**, 2325 (2004).